OBSERVATÓRIO NACIONAL (ON/MCTI)

DIVISÃO DE PROGRAMAS DE PÓS-GRADUAÇÃO

DISSERTAÇÃO DE MESTRADO

TOMOGRAFIA 2-D
DE TEMPOS DE PRIMEIRAS CHEGADAS
UTILIZANDO
O ALGORITMO GENÉTICO
COM ELITISMO

Aluno: Rodrigo Bijani Santos

Orientador: Cosme Ferreira da Ponte Neto

Rio de Janeiro

2012

Rodrigo Bijani Santos

Tomografia 2-D de tempos de primeiras chegadas utilizando o Algoritmo Genético com Elitismo

Dissertação apresentada ao Departamento de Geofísica do Observatório Nacional (ON/MCTI) para obtenção do título de Mestre em Geofísica
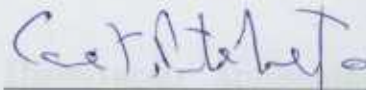
Orientador: Cosme Ferreira da Ponte Neto

Rio de Janeiro

2012

"TOMOGRAFIA 2-D DE TEMPOS DE PRIMEIRAS CHEGADAS UTILIZANDO O ALGORITMO GENÉTICO COM ELITISMO"

RODRIGO BIJANI SANTOS

DISSERTAÇÃO SUBMETIDA AO CORPO DOCENTE DO PROGRAMA DE PÓS-GRADUAÇÃO EM GEOFÍSICA DO OBSERVATÓRIO NACIONAL COMO PARTE DOS REQUISITOS NECESSÁRIOS PARA A OBTENÇÃO DO GRAU DE MESTRE EM GEOFÍSICA.

Aprovada por:

_____
Dr. Cosme Ferreira da Ponte Neto – ON/MCTI (Orientador)

_____
Dr. Irineu Figueiredo – ON/MCTI

_____
Dr. Wladimir Shukowsky – IAG/USP

RIO DE JANEIRO - BRASIL
16 DE FEVEREIRO DE 2012

Agradecimentos

Meus sinceros agradecimentos às pessoas que foram indispensáveis neste projeto:

Meu orientador Cosme Ferreira da Ponte Neto por todo o apoio, orientação, confiança e bons momentos de trabalho ;

Jandyr de Menezes Travassos pela ideia que iniciou este projeto e pela disponibilização dos dados de campo;

Constantino de Mello Motta pela substancial ajuda nas implementações computacionais;

Saulo Siqueira Martins pelo auxilio no processamento dos dados de campo;

Colegas de pós-graduação: Dionisio, Flora, Leonardo, Vanderlei e todos os outros. Não somente pelas discussões e sugestões mas também pelos momentos de descontração;

A amiga e namorada Jeannie, pelo carinho, discussões e apoio em todos os momentos.

E principalmente aos meus pais, Tania e Wenceslau, pela maravilhosa estrutura familiar, pelo eterno apoio e compreensão;

Sumário

Resumo

Tradicionalmente, a tomografia de tempos de primeiras chegadas é tratada como um problema inverso não-linear que é resolvido através de métodos determinísticos de otimização. Estes métodos minimizam funções-objetivo através do cálculo de suas derivadas. Em alguns problemas geofísicos, os cálculos das derivadas são computacionalmente dispendiosos e os métodos determinísticos tornam-se ineficazes. Outra limitação inerente aos métodos determinísticos está na forte relação entre o modelo inicial e o aprisionamento das soluções em mínimos locais. Para contornar essas limitações, nós aplicamos o Algoritmo Genético com Elitismo (AGE) ao problema da tomografia de tempos de primeiras chegadas em dados de Ground Penetrating Radar (GPR) adquiridos na geometria *cross-hole*. Simulando as etapas evolutivas de uma determinada espécie, este método heurístico localiza os possíveis mínimos globais no espaço de soluções sem calcular as derivadas da função objetivo, e sem depender do modelo inicial escolhido. Nós obtivemos bons resultados ao testarmos nosso método a dois conjuntos de dados sintéticos ruidosos. O primeiro simula um meio de camadas horizontais e o segundo consiste em meio homogêneo com uma anomalia isolada. Finalmente, a metodologia foi aplicada a um conjunto de dados de campo adquiridos na ilha de Florianópolis. Um padrão de estratos cruzados foi obtido na tomografia, o que está em concordância com a geologia local, cuja deposição sedimentar é fortemente dominada pela ação eólica. Métodos heurísticos aplicados a problemas geofísicos de grande dimensão apresentam bons resultados, porém são computacionalmente custosos. Esse fato sugere o acoplamento dos métodos heurísticos e determinísticos para explorar as potencialidades de cada técnica de otimização. Optamos por fazer o texto da dissertação na forma de uma publicação científica que compõe o corpo principal deste volume. Esta publicação científica foi submetida à revista Geophysical Prospecting em 16 de janeiro de 2012 e conta com a co-autoria de Saulo Siqueira Martins e Jandyr de Menezes Travassos.

Abstract

Traditionally, first-arrival travel time tomographic problems are treated as nonlinear inverse problems solved by deterministic optimization methods. These methods minimize the objective function by taking its derivatives. In some problems these derivatives are slow to compute and the method becomes inefficient. Another limitation inherent to deterministic methods is the strong relation between the starting model and local minima entrapment. To deal with these drawbacks, we apply a genetic algorithm with elitism (EGA) to cross hole tomography of Ground Penetrating Radar (GPR) data. Regardless the starting model, this heuristic method ideally finds the region of the solution space containing global minima without calculating derivatives. We obtain good results in applying our method in two noise-corrupted synthetic cross hole data sets. The first simulates horizontal strata and the second consists of a homogeneous background medium with single low-slowness anomaly. The methodology is also applied to in field data where a cross-strata pattern is achieved. This pattern is in accordance with the geological feature of the region. Heuristic methods applied to high-dimensional geophysical problems yield good results but are computationally expensive. Coupling heuristic and deterministic methods is recommended to exploit the full power of each optimization technique.

1 Introduction

Cross-hole first-arrival travel-time tomography was developed for the purpose of estimating the velocity distribution between parallel boreholes. In typical tomographic problems, the predicted data (travel-times) is calculated by a ray-tracing scheme (Fischer and Lees, 1993; Avendonk *et al.*, 2001; Bube and Langan, 2008). After that, the objective function (i.e., the mismatch between predicted and measured data plus regularization) is minimized throw some optimization technique to obtain a reasonably good velocity distribution.

Deterministic optimization methods are numerical techniques based on linear algebra concepts and derivative calculations whose purpose is to minimize functions. This class of methods is widely applied in tomographic problems mainly due to well established methods for stabilizing the multimodal objective functions encountered. A considered number of travel-time tomography methods based on deterministic techniques have been developed during the past years (Bois *et al.*, 1972; Scales, 1987; Phillips and Fehler, 1991; Moret *et al.*, 2004; Zhdanov *et al.*, 2006; Zhou *et al.*, 2008; Lelièvre *et al.*, 2011). Also belonging to this class of methods, of special attention is Aldridge and Oldenburg (1993) who present a two-dimensional tomographic inversion of travel time data using the Least-Squares estimator and the laplacian smoothness operator to minimize data misfit. To compute the travel-times they solve the eikonal equation using the Finite-difference method (Vidale, 1988). As opposed to Vidale (1988), Spoupios *et al.* (2001) use the shortest path method of Nakanishi and Yamagushi (1986) and Moser (1991) for the ray-tracing (i.e., the forward problem) and invert cross-hole and Vertical Seismic Profiling (VSP) data sets using Damped Least Squares. The linear systems are augmented to introduce smoothness constraints to the velocity distribution. Following the shortest path method approach, Becht *et al.* (2004) present an inversion strategy based on a simultaneous iterative reconstruction technique, in which the angular aperture of the ray-tracing is diminished until the number of travel-times of the smallest subset is sufficient to reconstruct a reasonably good image. Despite the large applicability, these deterministic methods applied to travel-time tomography present severe drawbacks associated with nonlinearity and irregularity of the tomographic objective function. These limitations promote local minima entrapment and a well suited starting model is required for good convergence. In some optimization problems, the

complexity of the objective function makes derivative calculations untreatable.

Another possibility to solve travel-time tomographic problems lies in the controlled random search optimization methods. These methods, also known as heuristic methods, prevent the local minima entrapment and promote a controlled search of the space of solutions. This random process, in some cases, simulates natural phenomena algorithmically, like Simulated Annealing (SA), Genetic Algorithm (GA) and Ant Colony Optimization. This algorithms have the capability of finding global minima in functions with multiple local minima regardless starting model. They are able to solve nonlinear and nonlocal optimization problems without the need for curvature information and, consequently, without the need for derivative calculations. These features can be particularly useful because they allow the use of fast approximate forward modelling, for which no exact derivative may be available. This results in a reduction of the computational effort. Although there are notable improvements in comparison with deterministic methods, the large dimensionality involved in most geophysical optimization problems can reduce the efficiency of heuristic methods. Furthermore, the stabilization of the tomographic objective function through regularization is usually difficult to implement. These drawbacks make the use of heuristic methods in geophysical inverse problems rare in the literature. Nevertheless, Boschetti *et al.* (1996) developed an inversion of seismic refraction data using genetic algorithms in a pseudo-subspace search method. They complemented the study by coupling heuristic and deterministic methods in their inversion scheme. Smith and Ferguson (2000) developed an interesting tomographic inversion of refracted seismic waves using Price (1977) algorithm. The model is specified as a two-dimensional assembly of polygonal bodies. The seismic velocities in these polygons maybe constant or may be defined as a function of depth or location. The parameters consist of the polygon vertex coordinates and velocity function coefficients. Velis (2001) utilized the Very Fast Simulated Annealing, implemented by Ingber (1989) to find the most promising areas in the solution space by inverting travel-times from 2-D anomalous structures.

We present the genetic algorithm with elitism (EGA) as the heuristic method for minimizing the tomographic objective function regardless the initial population. To achieve this goal, we construct a network with 226 nodes representing the interpretive model in which the

shortest path method of Nakanishi and Yamagushi, (1986) and Moser (1991) is applied for first-arrival travel-time calculation. This ray-tracing technique is fast and accurate given different velocity distributions. A brief discussion about the limitations of the shortest path method is also presented to complement the study on ray-tracing. We then apply the EGA as a tool for the Ground Penetrating Radar (GPR) tomography of first-arrivals. Starting from a random population, genetic algorithms progressively modifies the solution set by simulating the evolutionary behaviour of biological systems, until an acceptable result is achieved. Because of the strong ambiguity inherent in geophysical problems, the tomographic objective function is stabilized by a global-smoothness regularizing function. We test the potential and limitations of our method on noise-corrupted synthetic data and field data acquired at Florianopolis, Santa Catarina State, Brazil. We validate the final results using a statistical approach in which a series of inversions is processed to compute the average and the uncertainties of the estimated parameters.

2 Methodology

2.1 The cross-hole travel-time problem

Consider a two-dimensional rectangular region between two parallel wells. The Ground Penetrating Radar (GPR) measurements are accomplished by using a transmitting antenna (Tx) located in a borehole to emit a high-frequency electromagnetic pulse. The radiated pulse propagates within the medium, and is eventually recorded at a receiving antenna (Rx) located in another borehole a known distance away. During a cross-hole survey (i.e., a set of runs), the recording process is repeated for various Tx and Rx positions along the boreholes. This is done in order to have raypaths covering the whole area between the two boreholes. A Common approach is to retrieve the arrival time of the direct wave from a subsurface velocity distribution. The modelling procedure is based on the assumption that the travel time of a ray is the integral of the slowness along the raypath:

$$t(ray) = \int_{ray} s(x, z) dl \ \ ,$$ (2.1)

where $s(x, z)$ is the slowness (reciprocal velocity) at the point (x, z) and dl is the differential length along the raypath. Equation 2.1 shows a linear relation between the slowness and the travel-times. To solve Equation 2.1, we approximate the slowness distribution by an interpretive model consisting of a regular two-dimensional grid of M discrete points, each with a constant slowness value. These discrete points are henceforth referred to as nodes. Then, a network is formed when the nodes are connected. These connections are referred to as edges (black lines in Figure 1). The edges can bear different weights. In our case, the weight of the edges are calculated by Equation 2.2 (Figure 1).

In ray-tracing, the weight is the travel-time between two nodes. After switch the slowness distribution from continuous to discrete domain, Equation 2.1 becomes:

$$t(ray) = \sum_{i=1}^{n} \frac{(s_i + s_{i+1})}{2} d_j, \qquad j = 1, ..., 4 \tag{2.2}$$

where d_j is the distance between connected nodes, n is the number of nodes in the raypath, s_i and s_{i+1} are consecutive nodes in the raypath. Equation 2.2 shows that the raypath of least time is the sum of the travel times of each edge of the raypath. With this conception in mind, we are applying Fermat's principle during the ray-tracing to compute the first-arrival travel-times between source-receiver pairs. Hereinafter, the raypath is referred to as shortest path. The distance d_j is calculated by triangular geometry, as presented in Figure 2. The distance d_1 needs to be specified at the beginning of the network construction while d_2, d_3 and d_4 (Figure
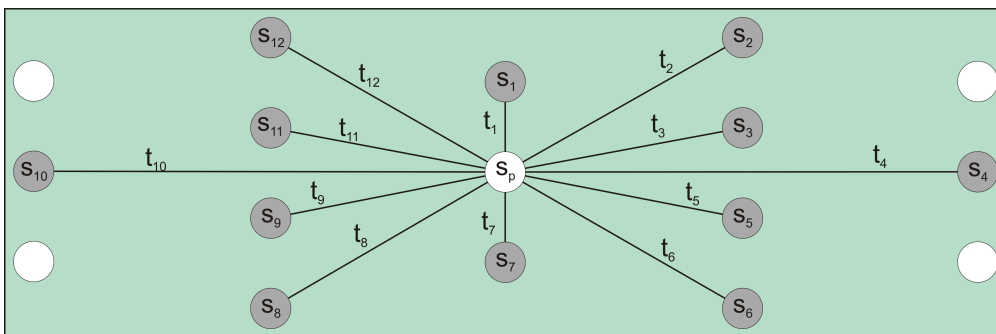

Figura 1: A clipping of the network to show how weigh the edges. Each node has a slowness value (s_1 up to s_{12}) and the travel-times between neighbouring nodes are calculated by Equation 2.2.
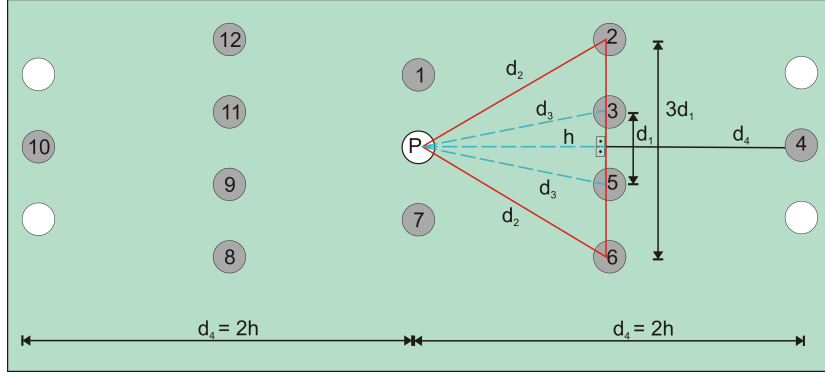
Figura 2: Edges construction. We use two isosceles triangles (blue dotted lines and red contiguous lines) to calculate the edges distances.

3) are calculated by the following expressions:

$$d_2 = \sqrt{\left(\frac{3d_1}{2}\right)^2 + h^2}, \tag{2.3}$$

$$d_3 = \sqrt{\left(\frac{d_1}{2}\right)^2 + h^2} \tag{2.4}$$

and

$$d_4 = 2h \tag{2.5}$$

where h is the height and d_1 is the base of the dotted triangle presented in Figure 2. The height of the dotted triangle is an input distance for the construction of the network, as well as the distance d_1.

The number of nodes in the network depends on the dimensions of the dotted triangle. The
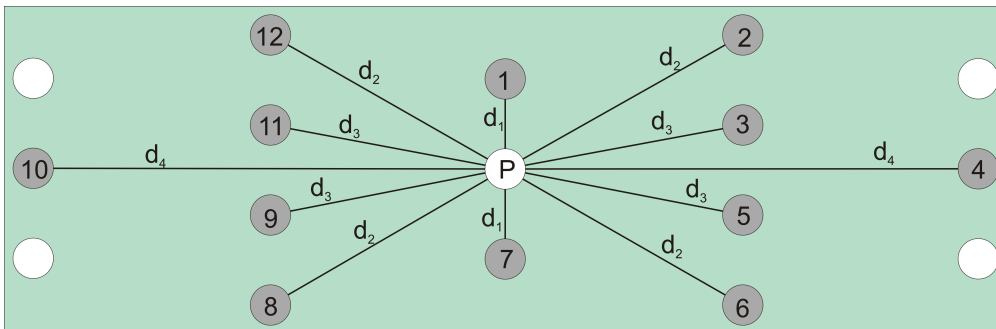

Figura 3: Second-level forward star. Twelve neighbouring nodes (gray) of node P (white) are numbered to show the clockwise connection. The nodes connection (edges) are represented by the distances d_1 up to d_4.

9

optimal configuration for the network is $h = d_1$, because this reduces its anisotropy. These issues will be treated in following section. Using a huge network increases the computation cost during the application of the shortest path method (Nakanishi and Yamagushi, 1986; Moser, 1991). The nodes of the slowness model are distributed regularly and each node is connected to its neighbouring nodes, just as shown in Figure 3. Our network is made exploiting the triangular geometry to get better angular discretization during network construction. This angular discretization allows more degrees of freedom finding the shortest path. The connection geometry presented in the Figure 3 is referred to as second-level forward star (Mak and Koketsu, 2011). After network construction, the shortest path method can be applied to compute the first-arrival travel times, which is based on Fermat's principle. The shortest path length algorithm used in this paper is implemented by Pape (1980) and based on Dijkstra (1959). This algorithm finds the shortest paths from a specific node to all other nodes in a network. The great advantage of Pape's (1980) algorithm is that errors in minimal travel-times are often corrected as soon as they are detected and not allowed to progress further.

2.2 Drawbacks of the shortest path method

Errors in the shortest path method are due to errors in the network geometry (Klimeš & Kvasnička, 1994) and errors in the heterogeneity of the network. A coarse network may poorly approximate slowness variations while a forward star with fewer neighbouring nodes results in an anisotropic raypath with poor degrees of freedom (Louis *et al.*, 2005). Figure 4a shows a typical example of a forward star with low-connectivity. Meanwhile, increasing the number of points in a network will not necessarily result in more accurate raypaths (Mak and Koketsu, 2011). The accuracy of the ray-tracing is only improved by using a forward star of higher level (i.e., each node is connected to farther nodes). Nevertheless, the excessive growth of the forward star level may cause errors in the calculation of the travel-times, since some nodes are no longer considered in the shortest path. Figure 4b shows a forward star with high-connectivity and longer edges, which promotes errors during the calculation of the minimum travel-time. We choose to use a second-order forward star with 12 neighbouring nodes and a network with 226 nodes and triangular geometry (Figures 3 and 5) respectively, to diminish the drawbacks of the
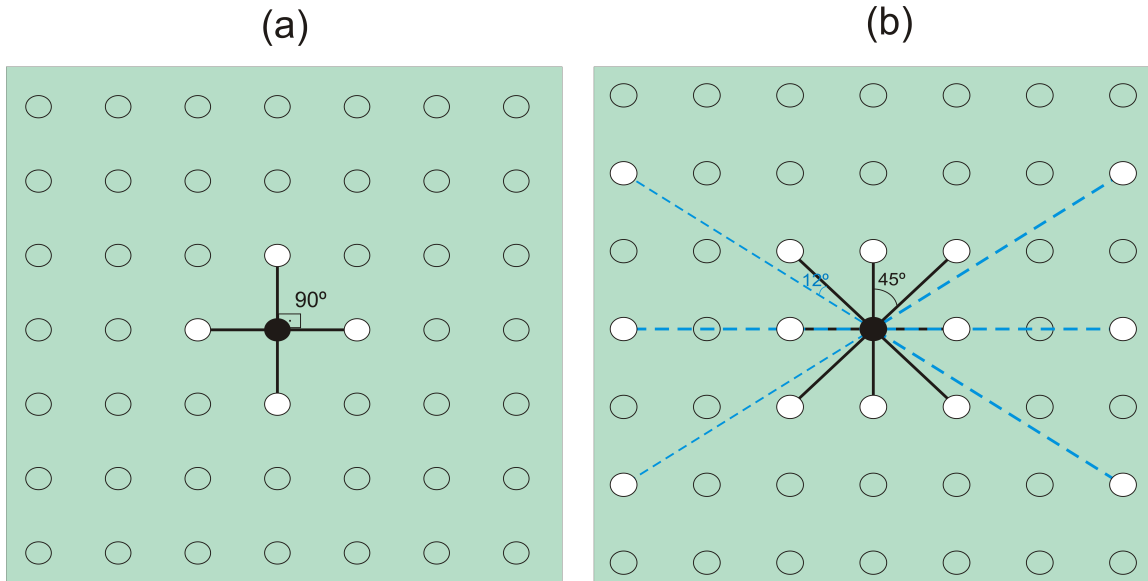
Figura 4: (a) Network geometry error. In this example we observe that the angles between edges are equal but the first-order forward star with only 4 neighbouring nodes promotes poor approximation of the shortest path.(b) Heterogeneity error. Longer edges (blue dotted lines) creates anisotropic raypaths. The angles between black edges and blues dotted edges are different, which is another indication of an anisotropic forward star.

shortest path method. For more detailed discussion on this issues see Fischer and Lees (1993),

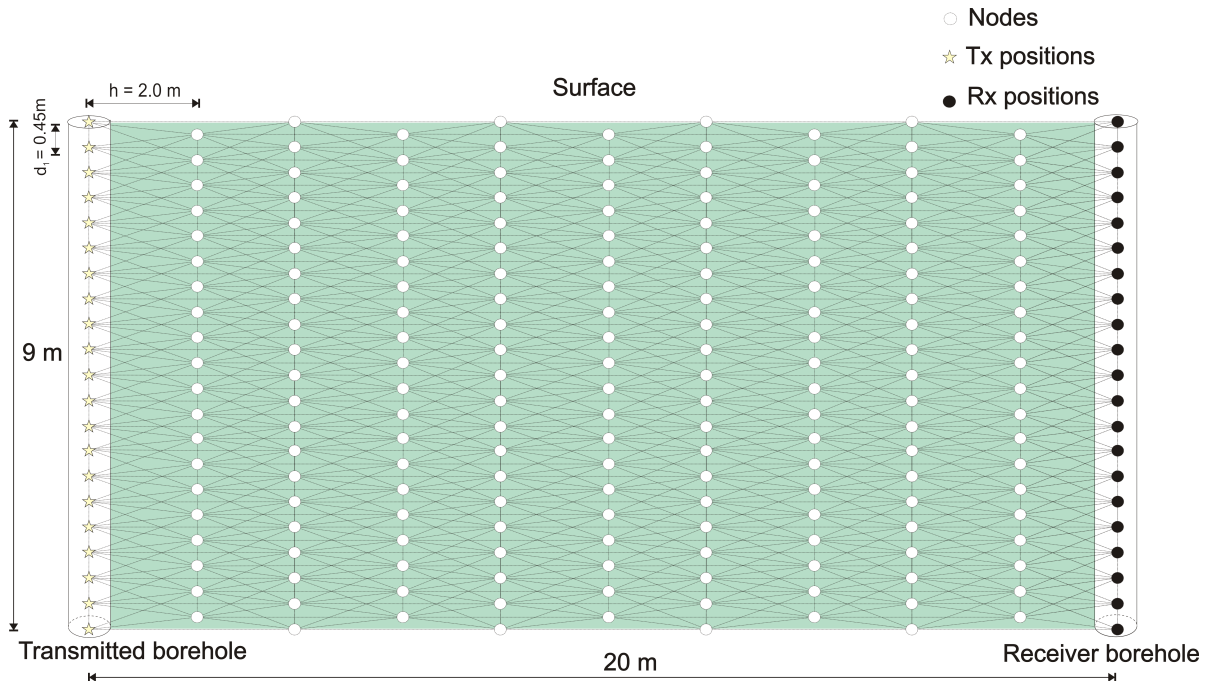Klimeš & Kvasnička (1994), Avendonk *et al.* (2001) and Louis *et al.* (2005).

Figura 5: Interpretive model sketch. Boreholes are 20 m apart and 9 m depth. The white circles, black circles and yellow stars are the 226 nodes of the slowness model. The distances h and d_1 are the input dimensions to the network construction. Black lines connecting the nodes are the edges of the network.

11

2.3 Inverse Problem

Let $\mathbf{t^{obs}}$ be a set of N first-arrival travel-times produced by an unknown slowness distribution in the subsurface. We want to estimate an M-dimensional vector $\mathbf{p}$ (i.e., parameters) of the slowness value of each node of the interpretive model (i.e., the network). To estimate the parameters in a stable way, we need to introduce *a priori* information about the slowness distribution. Traditionally, the *a priori* information incorporated in most geophysical inverse problems is the global smoothness of the spatial distribution of the physical property (Backus and Gilbert, 1968). This consists in requiring that each parameter p_i (estimated slowness of the i-th node) be as close as possible to parameter p_j (estimated slowness of an adjacent node either in x-or in the z-directions). We obtain a smooth estimate by minimizing the nonlinear objective function:

$$\phi(\mathbf{p}) = \frac{1}{N} \parallel \mathbf{t^{obs}} - \mathbf{t(p)} \parallel^2 + \lambda \frac{1}{M} \parallel \mathbf{Rp} \parallel^2 \tag{2.6}$$

where $\parallel \quad \parallel$ is the Euclidean norm, $\mathbf{t(p)}$ is an N-dimensional vector whose elements are the first-arrivals computed through the interpretive model, $\mathbf{R}$ is an NxM matrix representing the first-order difference operator of discrete derivatives in both the x- and z-directions and λ is a regularizing parameter, selected as the smallest positive value producing a stable solution. The regularizing parameter controls the tradeoff between the data misfit function (i.e., the first term of Equation 2.6) and the global-smoothness function (i.e., the second term in Equation 2.6). The addition of model-based constraints to the inverse problem is of upmost importance due to the inherent non-uniqueness and lack of stability of the travel-time tomographic problem.

2.4 Inversion Tool: Genetic Algorithm

Genetic algorithms consist of a random search algorithm based on the mechanics of natural selection and natural genetics (Goldberg, 1989). Genetic algorithms are widely used in linear and nonlinear optimization problems due to its capacity of finding the global minima of multimodal functions (Smith and Ferguson, 2000).

As in deterministic optimization methods, the genetic algorithms requires a set of initial

estimates (i.e., an initial population). The initial population can be randomly selected between a minimum and a maximum slowness value. The boundaries of the slowness values are referred to as search limits. The search limits plays a crucial role in the convergence of the genetic algorithms. If the search limits are too large, the genetic algorithms will need an equally large number of iterations (i.e., generations) to converge and the computational cost will make the problem intractable. Otherwise, if the search limits are wrongly set up, the genetic algorithms will converge to local minima that does not fit the data. These search limits can be used as a geological constraint.

The relevant stages in the implementation of the genetic algorithm, such as crossover, mutation and reproduction are widely discussed in Goldberg, (1989) and Boschetti *et al.*, (1996). We consider an extra stage in our implementation called elitism. At this stage, the fittest individual of the current generation is replicated to the next generation. The elitism can be considered as a convergence accelerator, because it allows the appearance of a "super-man" at the last generations. Genetic algorithms with this strategy are referred to as genetic algorithms with elitism or EGA (Chakraborty and Chaudhuri, 2003). We implement the EGA to minimize the nonlinear objective function (Equation 2.6) for some value of λ.

To check the stability of the estimates produced by the EGA, we use an elementary statistical analysis which consists in running a series of inversions by feeding the pseudo-random number generator with different seeds. This means that the initial population undergoes slight changes that promote slight differences in the estimates if the problem is well-regularized. Then we collect the best individual of each inversion and calculate the mean ($\overline{p_i}$) of each parameter of the interpretive model by the expression:

$$\overline{p_i} = \frac{1}{Q} \sum_{j=1}^{Q} p_i^j , \quad i = 1, ..., M \tag{2.7}$$

where Q is the number of inversions, p_i^j is the i-th parameter of the j-th inversion and and M is the number of parameters (slowness values) in the interpretive model. The uncertainties of every parameter are calculated as follows

$$\sigma_m^i \cong \frac{\sigma^i}{\sqrt{Q}} \quad , \quad Q > 4 \tag{2.8}$$

and

$$\sigma^i = \sqrt{\frac{1}{Q-1} \sum_{j=1}^{Q} (\overline{p_i} - p_i^j)^2} \quad , \quad i = 1, ...M \tag{2.9}$$

where σ^i is the sample standard deviation of each parameter, $\overline{p_i}$ is the mean of each parameter and p_i^j is the slowness value. Statistically, there is about 68% chance that p_i^j lies in the interval presented as follows (Young, 1962):

$$p_i^j = \overline{p_i} \pm \sigma_m^i \tag{2.10}$$

14

3   Results

Two numerical tests on synthetic data are undertaken to study the proposed methodology. The first synthetic data set is generated by a model of horizontal layers in which the slowness increases with depth (horizontal strata model). The second synthetic data set simulates an isolated buried geological body with anomalous slowness in a homogeneous slowness background (low-slowness anomaly model). For these tests, we use an interpretive model consisting of two ideal boreholes located 20 m apart and with 9 m depth, with twenty-one Transmission positions (Tx) in the transmission borehole and twenty-one Receiver positions (Rx) in the receiver borehole. The input distances for network construction are $d_1 = 0.45\ m$ and $h = 2.0\ m$. This configuration results in 441 shortest raypaths (i.e., 441 first-arrival travel-times) for the 226 unknown parameters (i.e., slowness of each node of the network). Figure 3 shows details of the interpretive model used in all tests. Our EGA was allowed to run for 1200 generations. When running on a computer with an Intel (R) Core (TM) i7-2600 CPU @ 3.40 GHz processor, the total time for inversion was approximately 12 h. In order to simulate a practical situation with noisy observed data, the synthetic data sets were contaminated with normally distributed pseudo-random noise with zero mean and standard deviation of $10^{-3}\ ns$. To check the stability of the estimates produced by the EGA, twenty inversion schemes with different initial populations are obtained by feeding the random number generator with different seeds. For all tests, an average slowness model and their uncertainties are computed to obtain the final results.

3.1 Horizontal strata model

Figure 6a shows the true slowness model that simulates horizontal strata in which the slowness values vary from 18.5 $(m/ns)^{-1}$ to 40.5 $(m/ns)^{-1}$. The true ray diagram is plotted in the background of Figure 6a to show the ray-coverage. As partial results, three of the twenty inverted slowness models and their respective ray diagrams are presented in Figure 6b-d. The initial population of each inversion is randomly selected between search limits 18.4 $(m/ns)^{-1}$ and 40.6 $(m/ns)^{-1}$. The objective function $\phi(\mathbf{p})$ (Equation 2.6) is minimized using regularization parameter $\lambda = 0.1$ and its convergence is plotted in Figure 6e. Although the inverted slowness models present small smeared features due to poor ray-coverage, the stratified pattern is observed in Figure 6b-d. These partial results suggests that the EGA has been able to find good individuals in the solution space. The good fitness between observed and predicted data (Figure 6f-h) confirms the good performance of the EGA facing this test. We present the average of the twenty inverted slowness models in Figure 7b and their respective uncertainties in Figure 7d. The small blurred features presented in Figure 7b-d are diminished in the average slowness model. The ray diagram in Figure 7b is in good accordance with that obtained in true model (Figure 7a).
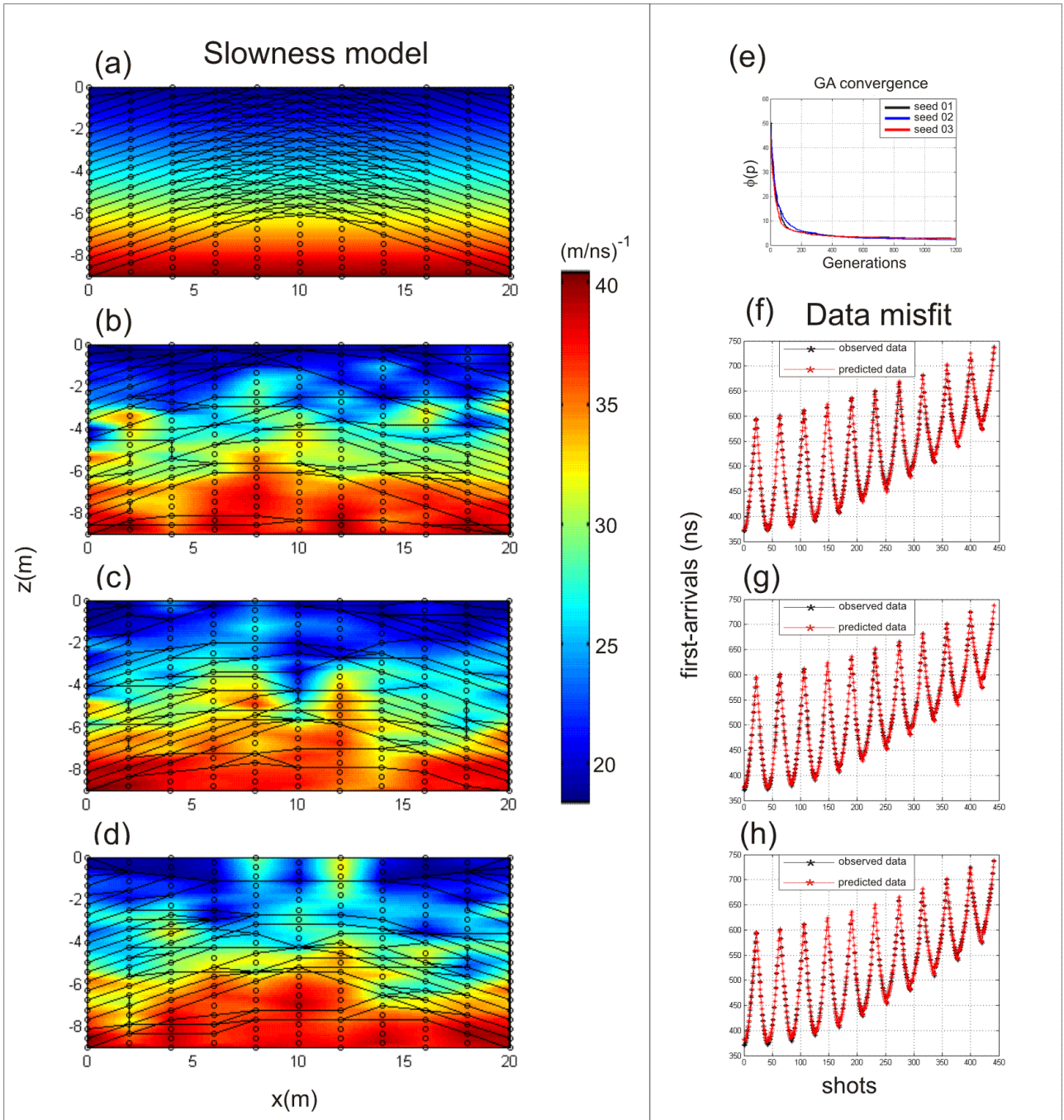
Figura 6: Partial results from horizontal strata model. (a) True slowness model and true ray diagram (shortest raypaths). Inverted slowness models and their respective ray diagrams from (b) seed 01, (c) seed 02 and (d) seed 03. Slowness values are indicated by the color bar. The circles in the whole slowness maps are the nodes of the interpretation model. The x-axis is the distance between wells and the z-axis is the wells depth. (e) The $\phi(\mathbf{p})$ convergence against the number of generations for each of the three inversions. Misfit versus the number of shots from seed 01 (f), seed 02 (g), seed 03 (h). The black asterisks are the first-arrivals from true slowness model and the red asterisks are the first-arrivals from the inverted slowness model.
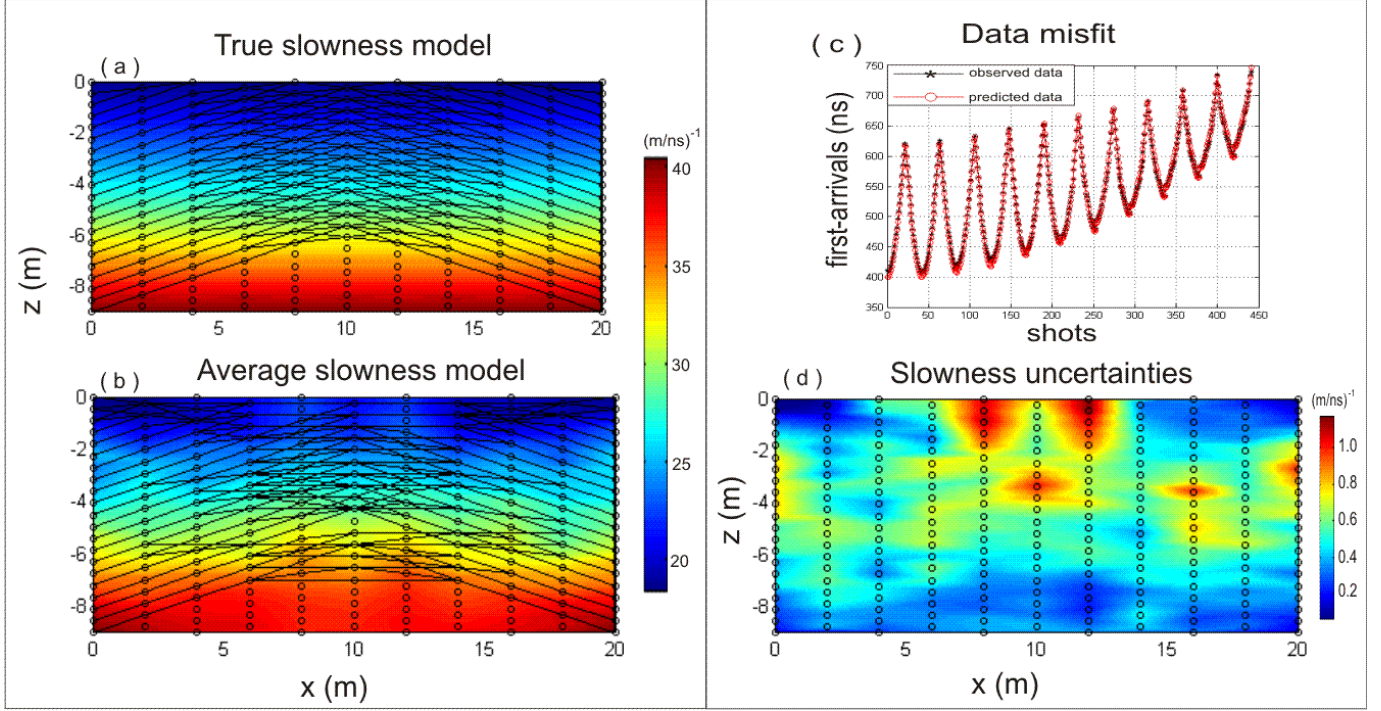
Figura 7: Final results from horizontal strata model. (a) true model, (b) average slowness model. The x-axis is the distance between wells and the z-axis is the wells depth. (c) Difference between observed and predicted data and (d) slowness uncertainties.

3.2 Low-slowness anomaly model

Figure 8a illustrates a low slowness anomaly model buried in the center of a constant-slowness background. The background slowness value is 18.5 $(m/ns)^{-1}$ and the slowness of the low slowness anomaly is 15.0 $(m/ns)^{-1}$. The objective function $\phi(\mathbf{p})$ (Equation 2.6) is minimized with $\lambda = 10$. The true ray-coverage is represented by the ray diagram in Figure 8a. The search limits for initial population selection are defined between 15.0 $(m/ns)^{-1}$ and 18.5 $(m/ns)^{-1}$. The partial results in Figure 8b-d present a low slowness anomaly without delineated borders. This means that the EGA succeeded in locating good individuals in this solution space. The global-smoothness function helps the EGA to converge to a relative stable solution. The ray-coverages of the partial results (Figure 8b-d) present small differences between the true raypaths. The misfits in Figure 8f-h are in good agreement with observed data. The average slowness model and its ray-diagram are presented in Figure 9b. As we can see, the low slowness anomaly was better delineated, but its slowness amplitude is slightly higher than in the true model. This means that another regularizing function should be considered. The red regions in the uncertainties map (Figure 9d) show that the EGA sensibility zone is directly related to the
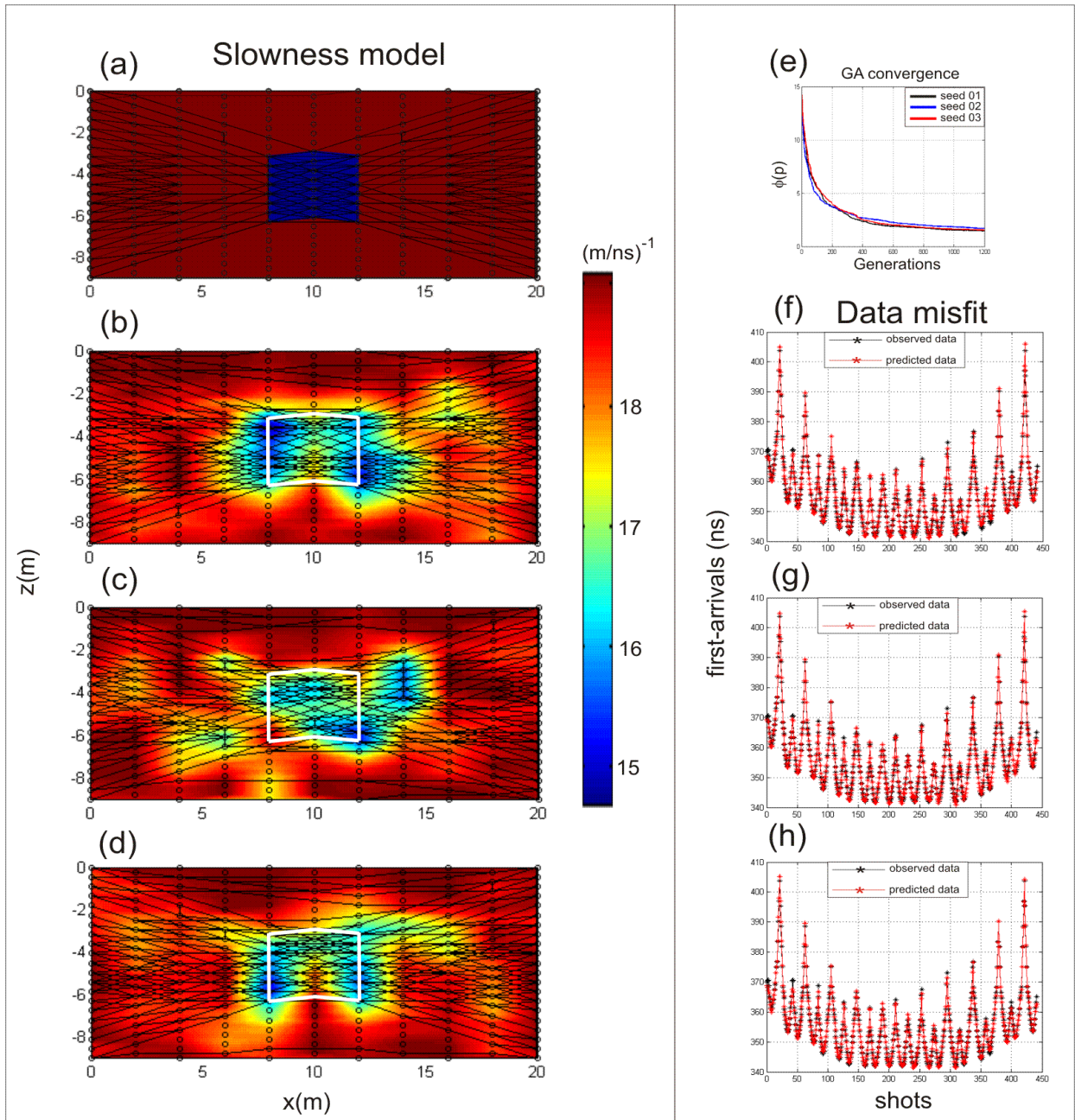
ray-coverage.

Figura 8: Partial results from low-slowness anomaly model. (a) True slowness model and true ray diagram (shortest raypaths). Inverted slowness models and their respective ray diagrams from (b) seed 01, (c) seed 02 and (d) seed 03. Slowness values are indicated by the color bar. The circles in the whole slowness maps are the nodes of the interpretation model. The white line in the center of the slowness maps represents the borders of the simulated geological body. The x-axis is the distance between wells and the y-axis is the wells depth. (e) The $\phi(\mathbf{p})$ convergence against the number of generations for each of the three inversions. Misfit versus the number of shots from seed 01 (f), seed 02 (g), seed 03 (h). The black asterisks are the first-arrivals from true slowness model and the red asterisks are the first-arrivals from the inverted slowness model.
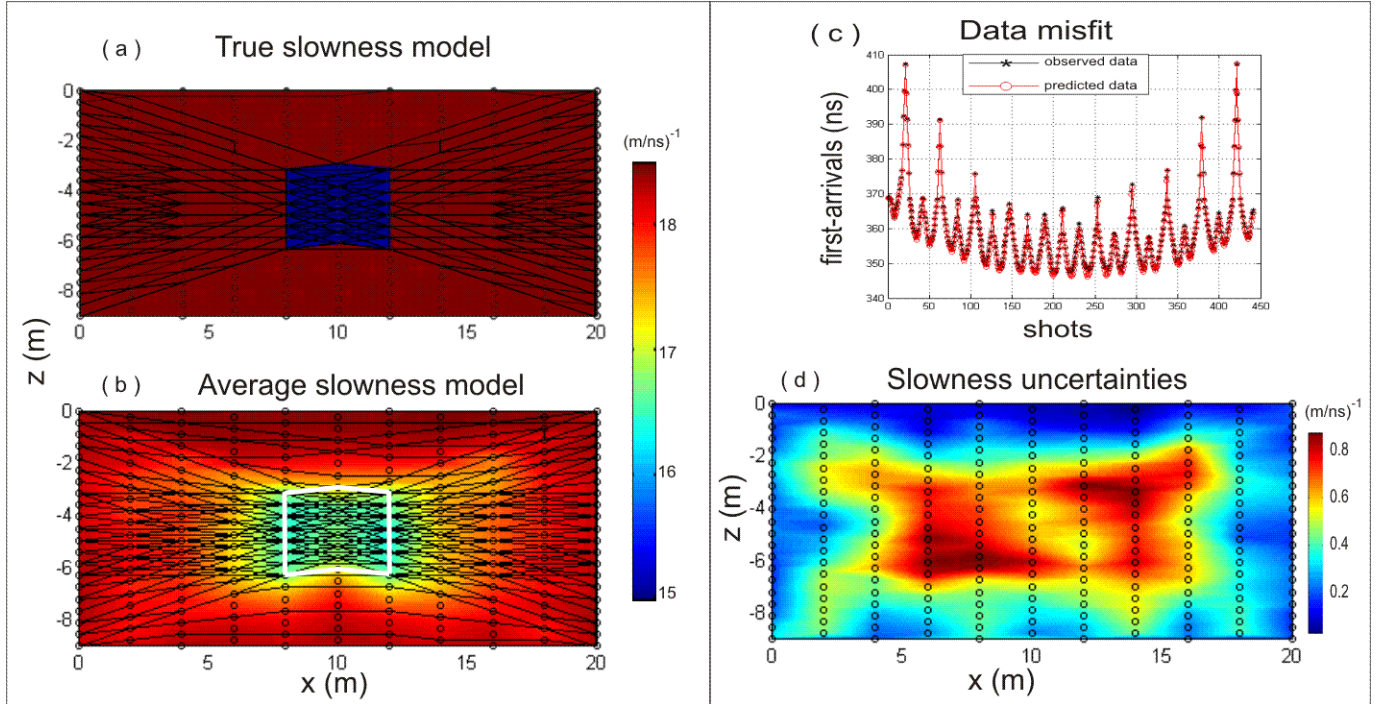
Figura 9: Final results from low-slowness anomaly model. (a) true model, (b) average slowness model. The white line in the center of the slowness maps represents the borders of the simulated geological body. The x-axis is the distance between wells and the z-axis is the wells depth. (c) Difference between observed and predicted data and (d) slowness uncertainties.

3.3   Application to field data

Following the experiments on synthetic data, we apply the proposed methodology on data sets acquired in a region of the island of Florianopolis, in Santa Catarina, Brazil. The local geology is composed of unconsolidated sandy deposits of mixed origin: marine, fluvial and eolic. The soil is a gray-brownish fine sand with less than 5% of silts and clay woth a hydraulic flux of 2.8 m/yr and an effective porosity of 0.2 (Conceição et al., 2007). It is a region heavily weathered by wind action, which promotes cross-strata sedimentation. Cross-strata are strata that are inclined with respect to a thicker stratum within which they occur. Cross-strata are commonly seen in river deltas, streams segments and beaches (Skinner and Porter, 1987).

The cross-well acquisition geometry consists on a survey with 46 runs in which the measurement points are spaced 0.2 m apart in both wells. This configuration provides a set of 2123 travel-times. The MALA equipment was used with a time window of 700 ns and 100 MHz frequency. The interpretive model is the same as the one applied on synthetic cases. We interpolate the raw data to match the positions of the antennas to the proposed interpretive

model. The two initial runs in the survey are discarded due to the proximity of the transmitter to the borehole mouth (Conceição et al., 2007).

We allowed the EGA to perform 2000 generations with $\lambda = 0.1$ and search limits defined between 16.6 $(m/ns)^{-1}$ and 25.0 $(m/ns)^{-1}$. The partial results are presented in Figure 10. Although the high noise in the data has led to some artifacts, the three inverted slowness models in Figure 10a-c present a cross-strata pattern. The data misfit presented in Figure 10d-f reveals a mismatch between observed and predicted data for the last shots, which is related to errors in the ray-tracing. The average slowness model presented in Figure 11a shows a rise on the cross-strata pattern. Figure 11c shows an over-predicted data, i.e., the observed data (black asterisks) are smaller than predicted data (red circles). This behaviour is probably related to a coarse discretization of the interpretive model.
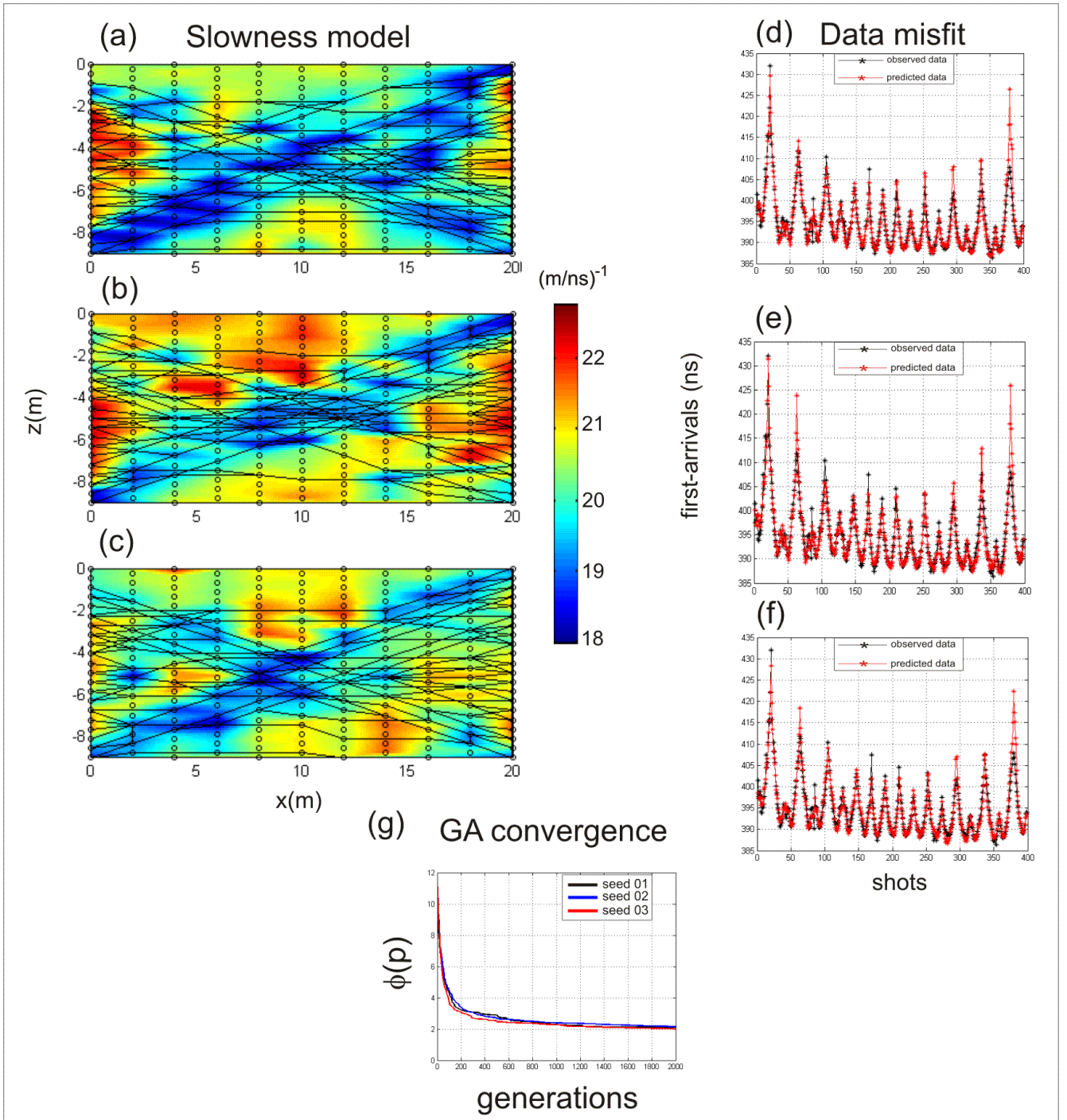
Figura 10: Partial results from field data. Inversion results and ray diagram from (a) seed 01, (b) seed 02, (c) seed 03. Slowness values are indicated by the color bar. The circles in the whole slowness maps are the nodes of the interpretive model. Misfit between observed and predicted data from (d) seed 01, (e) seed 02, (f) seed 03(g). The $\phi(\mathbf{p})$ convergence against the number of generations for each of the three inversions.
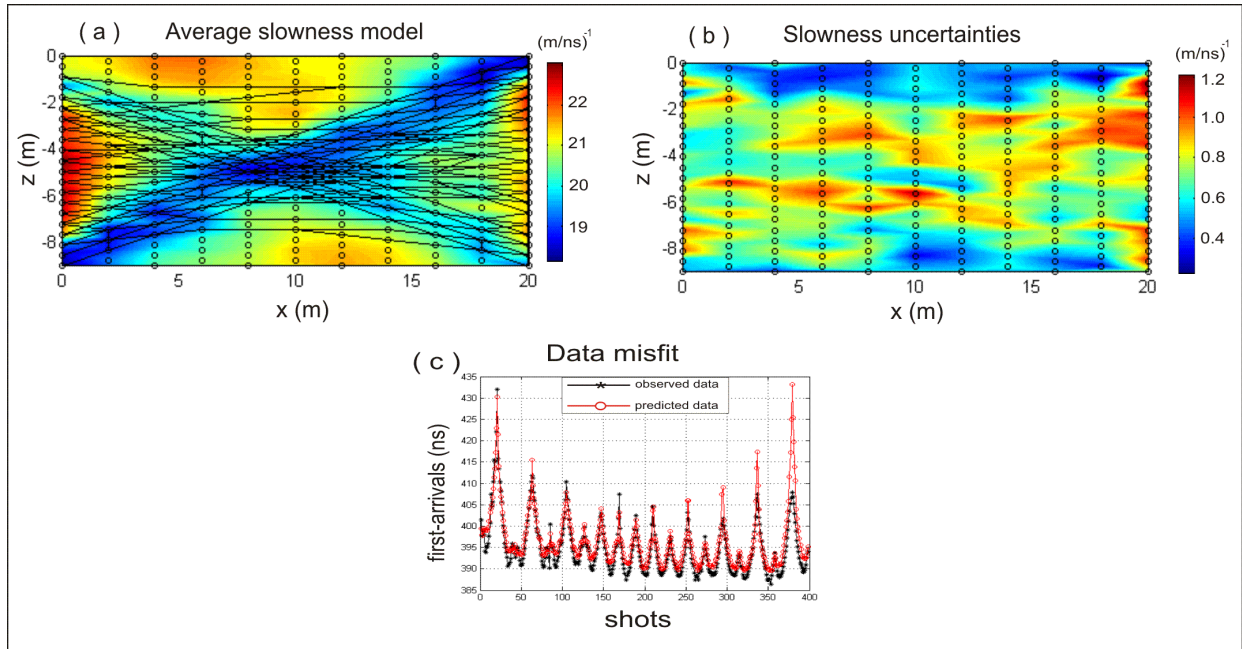
Figura 11: Final results from field data. (a) average slowness model with ray diagram, (b) slowness uncertainties map and (c) Misfit between observed and predicted data.

4   Conclusions

We have presented a genetic algorithm with elitism (EGA) for a cross-hole travel-time tomography which incorporates an efficient shortest path method in conjunction with a regularized inversion approach. The 2-D shortest path method is well suited to compute the first-arrivals accurately and in a rapid fashion. Despite of small heterogeneities in the interpretive model, the inverted ray-diagrams presented similarities to the true ray-diagrams.

The EGA proved to be powerful in minimizing multimodal functions regardless the starting model. However, it required a huge number of generations to achieve good convergence. This limitation suggests that the combination of heuristic and deterministic methods could be used as an optimal inversion tool. Taking the average of the inverted seems to smooth the blurred features in the all inverted slowness models. The uncertainty maps show the sensitivity zones of the EGA.

The EGA requires appropriate search limits to reconstruct slowness models that fit the data. We have also demonstrated that our algorithm is capable of producing reasonable slowness models using two different noise-corrupted synthetic data sets.

The results obtained by applying the methodology to field data showed that a coarse inter-

23

pretive model promotes a slight mismatch between observed and predicted data. Nevertheless, the interpretation is in concordance with the geological aspects of the region.

5   Acknowledgments

Referências

Aldridge, D.F., Oldenburg, D.W., 1993. Two-dimensional tomographic inversion with finite-difference traveltimes: Journal of Geophysics Exploration, **2**: 257-274.

Avendonk, H.J.A., Harding, A.J., Orcutt, J.A., Holdbrook, W.S., 2001. Hybrid shortest path and ray bending method for traveltime and raypath calculations: Geophysics, **66**, 648-653.

Backus, G.E., Gilbert, F., 1968. The Resolving power of Gross Earth Data: Geophysical Journal of the Royal Astronomical Society, **16**: 169â205.

Becht, A., Tronicke, J., Appel, E., Dietrich, P., 2004. Inversion strategy in crosshole radar tomography using information of data subsets: Geophysics, **69**, 222-230.

Bois, P., Porte, M.L., Lavergne, M., Thomas, G., 1972. Well-to-well seismic measurements, Geophysics, **37**, 471-480.

Boschetti, F., Dentith, M.C., List, L.D., 1996. Inversion of seismic refraction data using genetic algorithms: Geophysics, **61**, 1715-1727.

Bube, K.P., Langan, R.T., 2008. A continuation approach to regularization of ill-posed problems with application to crosswell-traveltime tomography: Geophysics, **73**: VE337-VE351.

Chakraborty, B., Chaudhuri, P., 2003. On The use of Genetic Algorithm with Elitism in robust and nonparametric multivariate Analysis: Austrian Journal of statistics, **32**, 13-27.

Conceição, E., Ribeiro, C.G., Travassos, J.M., 2007. 1-D Analysis of EM Wave Velocity between two boreholes: 10th International Congress of The Brazilian Geophysical Society, Rio de Janeiro, Brasil, Expanded Abstracts.

Dijkstra, E.W., 1959. A note on two problems in connection with graphs: Numer. Math., 269-271.

Fischer, R., Lees, J.M., 1993. Shortest path ray tracing with sparse graphs: Geophysics, **58**, 987-996.

Goldberg, D.E., 1989, Genetic algorithms in search, optimization, and machine learning: Addison-Wesley Publ. Co., Inc. ISNB: 0-201-15767-5.

Ingber, L., 1989. Simulated annealing-Practice versus theory: Journal of Mathematical Computer Modeling, **18**, 29â57.

Klimeš, L., Kvasnička, M., 1994. 3D network ray tracing: Geophysical Journal International, **116**, 726-738.

Lelièvre, P.G., Farquharson, C.G., Hurich, C.A., 2011. Inversion of first-arrival seismic traveltimes without rays, implemented on unstructured grids: Geophysical Journal International, **186**, 1-15.

Mak, S., Koketsu, K., 2011. Shortest path ray tracing in cell model with a second-level forward star: Geophysical Journal International, **186**, 1279-1284.

Moret, G.J.M., Clement, W.P., Knoll, M.D., Barrash, W., 2004. VSP traveltime inversion: Near-surface issues: Geophysics, **69**, 345-351.

Moser, T.J., 1991. Shortest path calculation of seismic rays: Geophysics, **56**, 59-67.

Nakanishi, I., Yamagushi, K., 1986. A numerical experiment on nonlinear image reconstruction from first-arrival times for two-dimensional island arc structure: Journal of Physics of the Earth, **34**, 195-201.

Pape, U., 1980. Shortest Path Lengths: Transactions on Mathematical Software, **6**, 450-455.

Phillips, W.S., Fehler, M.C., 1991. Traveltime tomography: A comparison of popular methods: Geophysics, **56**, 1639-1649.

Price, W. L., 1977. A controlled random search procedure for global optimization: Comp. J., **20**, 367â370.

Scales, J.A., 1987. Tomographic inversion via the conjugate gradient method: Geophysics, **52**, 179-185.

Skinner, B.J., Porter, S.C., 1987. Physical Geology: John Wiley & Sons, Inc. ISNB: 0-471-05668-5.

Smith, D.N., Ferguson, J.F., 2000. Constrained inversion of seismic refraction data using the controlled random search: Geophysics, **65**, 1622-1630.

Soupios, M.P., Papazachos, C.B., Juhlin, C., Tsokas, G.N., 2001. Nonlinear 3-D traveltime inversion of crosshole data with an application in the area of the Middle Ural Mountains: Geophysics, **66**, 627-636.

Vasco, D.W., Peterson Jr., J.E., Lee, K.H., 1997. Ground-penetrating radar velocity tomography in heterogeneous and anisotropic media: Geophysics, **62**, 1758-1773.

Velis, D.R., 2001. Traveltime inversion for 2-D anomaly structures: Geophysics, **66**, 1481-1487.

Vidale, J.E., 1988. Finite-difference calculation of travel times: BSSA, **78**, 2062-2076

Young, H.D., 1962. Statistical treatment of experimental data: McGraw-Hill, New York.

Zhou, B., Greenhalgh, S., Green, A., 2008. Nonlinear traveltime inversion scheme for crosshole seismic tomography in tilted transversely isotropic media: Geophysics, **73**, D17-D33.

Zhdanov, M.S., Vignoli, G., Ueda, T., 2006. Sharp boundary inversion in crosswell travel-time tomography: Journal of Geophysics and Engineering, **3**, 122-134.